SANDIA REPORT

SAND2011-7778
Unlimited Release
Printed October 2011

Pyrometry simulator (`pyrosim`) for diagnostic design

Daniel H. Dolan

Prepared by
Sandia National Laboratories
Albuquerque, New Mexico 87185 and Livermore, California 94550

Sandia National Laboratories is a multi-program laboratory managed and operated by Sandia Corporation, a wholly owned subsidiary of Lockheed Martin Corporation, for the U.S. Department of Energy's National Nuclear Security Administration under contract DE-AC04-94AL85000.

Issued by Sandia National Laboratories, operated for the United States Department of Energy by Sandia Corporation.

Available to DOE and DOE contractors from
U.S. Department of Energy
Office of Scientific and Technical Information
P.O. Box 62
Oak Ridge, TN 37831

Telephone: (865) 576-8401
Facsimile: (865) 576-5728
E-Mail: reports@adonis.osti.gov
Online ordering: http://www.osti.gov/bridge

Available to the public from
U.S. Department of Commerce
National Technical Information Service
5285 Port Royal Rd
Springfield, VA 22161

Telephone: (800) 553-6847
Facsimile: (703) 605-6900
E-Mail: orders@ntis.fedworld.gov
Online ordering: http://www.ntis.gov/help/ordermethods.asp?loc=7-4-0#online

SAND2011-7778
Unlimited Release
Printed October 2011

Pyrometry simulator (`pyrosim`) for diagnostic design

Daniel H. Dolan
Sandia National Laboratories
P.O. Box 5800
Albuquerque, NM 87185-1195

Abstract

Signal estimates are crucial to the design of time-resolved pyrometry measurements. These estimates affect fundamental design decisions, including the optical relay (fiber versus open beam), spectral range (visible or infrared), and amplification needs (possibly at the expense of time resolution). The `pyrosim` program makes such estimates, allowing the collected power, photon flux, and measured signal to be determined in a broad range of pyrometry measurements. Geometrical collection limits can be applied; sample emissivity, transfer efficiency, and detector sensitivity may also be specified, either as constants or functio ns of wavelength.

Acknowledgments

The `pyrosim` program and the examples presented in this report are the result of many conversations with Tom Bergstresser, David Holtkamp, David Partouche, Achim Seifter, and Tom Ao. Portions of the program were developed under Sandia LDRD 79877.

The quantum efficiency plot shown in Figure 5 is derived from measurements taken by Sheri Payne at National Security Technologies.

Contents

Figures

Tables

This page intentionally left (almost) blank.

1 Background

Optical pyrometry is the measurement of temperature using the intrinsic radiation produced by objects above absolute zero. The fundamental principles of this radiation have been understand for over a century [1], yet pyrometry measurements are complicated by numerous subtleties. Hot objects generally radiate more light than cold objects, and increasing temperatures shifts larger fractions of this radiation to shorter wavelengths, but such generalities can be misleading. The design and operation of pyrometers depends on specific performance criteria: what temperature range is measurable, and how sensitive is a particular pyrometer in this range?

Many factors affect the design of an optical pyrometer, but chief among them is the wavelength range. This choice is intrinsically linked to the temperature range of interest. Theoretically, human body temperature could be inferred from trace visible emission, but in practice infrared measurements are much more feasible; conversely, eV temperature measurements would be poorly served by infrared pyrometers, while visible (perhaps even ultraviolet to x-ray) measurements would be more appropriate. Wavelength range affects virtually all aspects of pyrometer design: light collection/transfer, detector, limiting speed, cost, and so on.

Performance projections, based on wavelength range and other factors, are useful in determining whether a costly design choice provides significant improvements. The `pyrosim` program was developed to provide these projections, delivering rapid assessments of pyrometer design. Varying levels of detail can input into the program to refine these estimates, generating order of magnitude projections, precise calibration data, or anything in between. Calculation accuracy depends upon the user's level of interest in characterizing a real pyrometer. Portions of this calculation can be obvious—measurements with 50% emissivity yield half the signal of that from a black body—but the program provides a framework for much more complex situations. Spectral variations in emissivity, relay efficiency, and detector sensitivity are supported in `pyrosim` to handle situations where human intuition is not always reliable, particularly for pyrometers that operate over wide spectral bands.

The remainder of this report is organized as follows. Section 2 provides a brief theoretical background, documenting notational conventions. Section 3 describes the use of `pyrosim`, both the graphical interface and as a MATLAB function. Section 4 provides several program examples for training purposes. Section 5 summarizes the report.

2 Theory

Figure 1 shows a conceptual layout of a pyrometry measurement. Light generated by a sample at temperature T is collected by an optical relay and carried to a detector. For purpose of this discussion, the sample temperature is assumed to constant and spatially uniform throughout the measurement. The sample has an emissivity ϵ related to its reflectivity and transparency by Kirkoff's law [2]. The optical relay defines a limiting collection

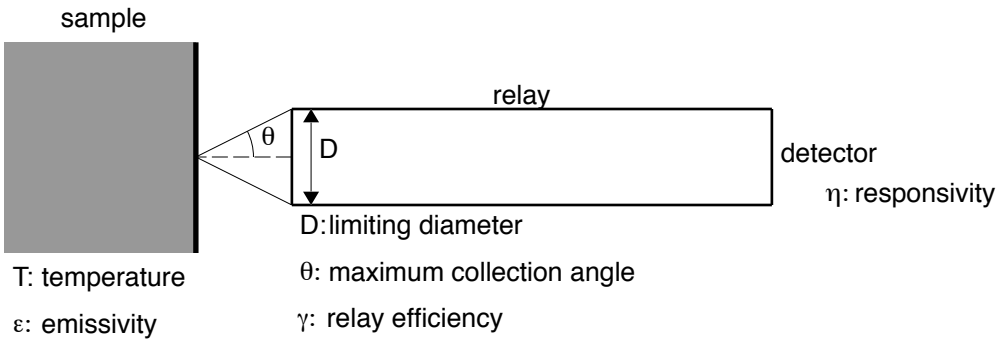

Figure 1. Pyrometry measurement layout

diameter D and collection angle θ (from the normal), assuming that the relay is overfilled by radiation from the sample. Light passes through the relay with efficiency $\gamma \leq 1$ to reach a detector with responsivity η. Geometric light collection (diameter and maximum angle) are assumed to be constant at all wavelengths, but all remaining parameters (ϵ, γ, and η) may be wavelength dependent.

The spectral radiance (power per unit area per unit solid angle per unit wavelength[1]) L generated by a Lambertian emitter is:[2]

$$\frac{dL}{d\lambda} = \epsilon(\lambda)\frac{2hc_0^2}{\lambda^5\left(\exp(hc_0/\lambda k_B T) - 1\right)} \tag{1}$$

where h is Plank's constant ($4.135667516 \times 10^{-15}$ eV·s), c_0 is the vacuum speed of light (2.99792458×10^8 m/s), and k_B is Boltzman's constant (8.6173324×10^{-5} eV/K). The spectral power Φ collected by the pyrometer is:

$$\frac{d\Phi}{d\lambda} = \left(\frac{\pi D \sin\theta}{2}\right)^2 \gamma(\lambda)\ \frac{dL}{d\lambda}. \tag{2}$$

The total collected power is determined by integration over all relevant wavelengths:

$$\Phi = \int_{\lambda_1}^{\lambda_2} \frac{d\Phi}{d\lambda}\, d\lambda \tag{3}$$

accounting for emissivity and relay efficiency variations as needed.

While most laboratory measurements are based on the wavelength scale (typically micrometers), it is numerically convenient to integrate with respect to photon energy $E \equiv hc_0/\lambda$. The spectral radiance is now:

$$\frac{dL}{dE} = \epsilon(E)\frac{AE^3}{e^{E/k_B T} - 1} \to \epsilon(Ak_B T)E^2 \quad (E \to 0) \tag{4}$$

[1] All wavelengths in this work are referenced to vacuum.

where $A = 2/h^3c_0^2$. The negative sign in translating from wavelength to photon energy is incorporated into the integration of total power, moving from minimum to maximum photon energy rather than minimum to maximum wavelength (as in Equation 3)

$$\Phi = \int_{E_1}^{E_2} \frac{d\Phi}{dE}\, dE \tag{5}$$

Emissivity and relay variations are now expressed in terms of photon energy rather than wavelength.

Other pyrometric quantities can be calculated in a similar fashion as Equation 5. For example, the number of collected photons Φ_N is simply a scaling of power by photon energy.

$$\Phi_N = \int_{E_1}^{E_2} \frac{1}{E}\frac{d\Phi}{dE}\, dE \tag{6}$$

The electrical signal S from a pyrometer is proportional to spectral power (integrated over all photon energies).

$$S = \int_{E_1}^{E_2} \eta(E)\frac{d\Phi}{dE}\, dE \tag{7}$$

The responsivity η of the pyrometry may vary with photon energy, so it should be incorporated within the integral.

3 Using the `pyrosim` program

Version 1.1 of the `pyrosim` program was created in MATLAB 2009b and should operate in all later releases; compiled versions, which run outside of MATLAB, are available upon request. Individuals outside Sandia interested in using `pyrosim` should contact the author for a license.

Running `pyrosim` without any input arguments in MATLAB:

```
>> pyrosim
```

or outside of MATLAB launches a graphical interface for the program. Passing input arguments in MATLAB:

```
>> power=pyrosim('temperature',1000);
```

bypasses the graphical interface, returning results in one (or more) function outputs. Details of each interface are given below. A brief summary may obtained by typing `help pyrosim` at the MATLAB command line.

Figure 2 shows the `pyrosim` graphical interface, which contains the input panel, the results table, the results plot, the graphic toolbar, and the program menu. All aspects of the

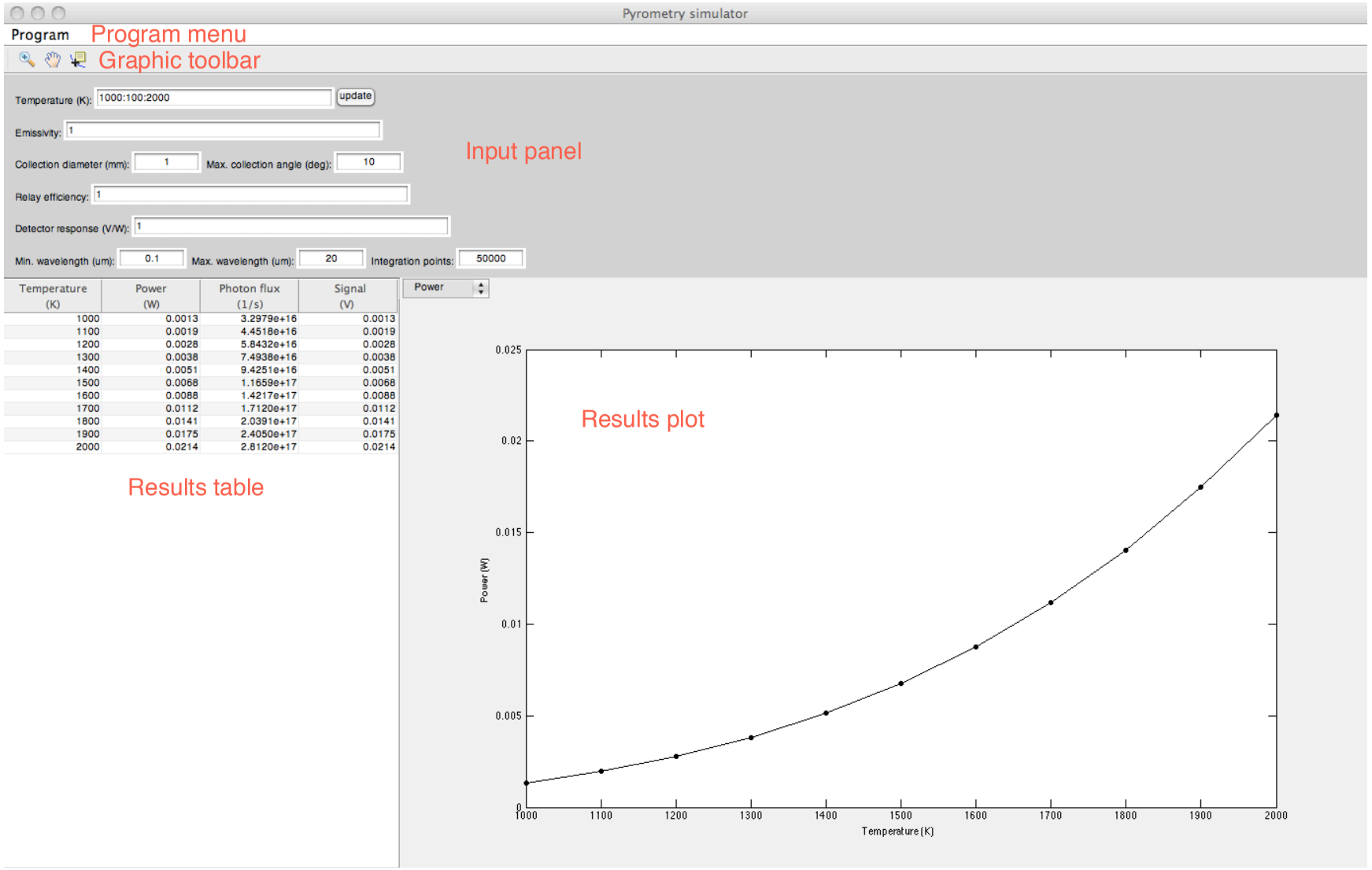

Figure 2. Graphical interface for `pyrosim`

pyrometry simulation are defined in the input panel. Default values are loaded into the input panel at startup and can be changed at any time; pressing the "update" button runs a new calculation and refreshes the results table and plot. The results table shows the calculated power (W), photon flux (1/s), and electrical signal (V) for the defined pyrometer at each specified temperature. The results plot shows a graphical representation of the calculation specified in the popup box at the top left corner; right clicking on the plot allows selection of linear or logarithmic scaling for each plot axis. The graphic toolbar provides interactive plot manipulation, using standard MATLAB functions (zoom, pan, and data cursor) to change the appearance (but not the content) of the results plot. The program menu provides information about `pyrosim`, exports results to a file, and terminates the program.

Table 1 summarizes the inputs available to the graphical and functional interfaces of `pyrosim`. Most of the inputs are self explanatory, but a few features merit further description.

- MATLAB style temperature inputs are supported. The simplest example is single temperature span: `1000:100:2000`, which starts at 1000 and increases in increments of 100 up to maximum possible value of 2000. Multiple temperature spans can be also specified (*e.g*, `1000:100:2000 3000:1000:10000`), but square brackets (`[1000:100:2000 3000:1000:10000]`) are required in the functional interface.

- The emissivity, relay efficiency, and response inputs can accept three different input types: a single number, a $N \times 2$ array (functional interface only), or a file name containing tabular data. In the latter case, the file should contain two numerical columns, separated by white space, defining the wavelength and value (emissivity, efficiency, or response); any header prior to the column is ignored. The following example defines perfect relay efficiency in the visible spectrum with zero efficiency outside this range.

  ```
  Wavelength (um)     Efficiency (-)
  0.39                 0.0
  0.40                 1.0
  0.70                 1.0
  0.71                 0.0
  ```

  Coarse tabulations are acceptable—`pyrosim` will interpolate the table onto the integration grid as necessary. Values outside the table range are automatically set to zero.

- The maximum wavelength may be any positive number up to and including infinity (`inf`), but the minimum wavelength must be greater than zero. The number of wavelengths should be chosen to prevent large variations in the user functions (emissivity, relay, and efficiency) or Equation 3; larger numbers improve integration accuracy, but may slow down calculations over many temperature or wavelength regions. A good rule of thumb is to keep average wavelength interval at 0.01 μm or lower.

- The results table (and data exported from the graphical interface) is displayed with MATLAB's "short" format (4–5 significant digits). The functional interface maintains

Table 1. `pyrosim` function inputs

Parameter (Units)	Acceptable values	Default value
`temperature` (K)	Array of positive numbers	1000
`emissivity` (-)	Single number, $N \times 2$ array, or file name	1
`diameter` (mm)	Single number	1
`max_angle` (deg)	Single number	10
`relay` (-)	Single number, $N \times 2$ array, or file name	1
`response` (V/W)	Single number, $N \times 2$ array, or file name	1
`min_wavelength` (μm)	Single number	0.1
`max_wavelength` (μm)	Single number	20
`num_wavelength` (μm)	Single number	50,000

roughly nine significant digits, a limitation of the fundamental constants h, c_0, and k_B. Either format is sufficient for most applications, but precise comparisons between `pyrosim` and theoretical predictions (such as the Stefan-Boltzman law) should use the functional mode.

4 Examples

The following examples illustrate the validity and practical use of `pyrosim`. The first example compares `pyrosim` calculations to the Stefan-Boltzman law. Next, several infrared band pyrometry calculations are considered to demonstrate the temperature range and sensitivity of different wavelength ranges. Finally, a visible pyrometry measurement via a streaked spectrometer is considered.

4.1 Validation

The total exitance (power per unit area) of a blackbody is given by the Stefan-Boltzman law:

$$M \equiv \frac{\Phi}{A} = \sigma T^4 \tag{8}$$

where σ is 5.67037×10^{-8} W/m^{-2}·K^4. This relationship follows from integration of Plank's law (Equation 1) over all wavelengths and solid angles. A numerical estimate for exitance can be made with `pyrosim`, evaluating the power in a semi-infinite wavelength region for a maximum collection angle of 90° with an arbitrary collection diameter (say 1 mm); dividing this power by the corresponding area yields values for M at discrete temperature values.

Figure 3 compares two `pyrosim` calculations with the Stefan-Boltzman law. Both calculations are very similar to the theoretical curve: below 5000 K, the agreement is better than 1 ppm. At higher temperatures, however, the calculations diverge from theory, which is a

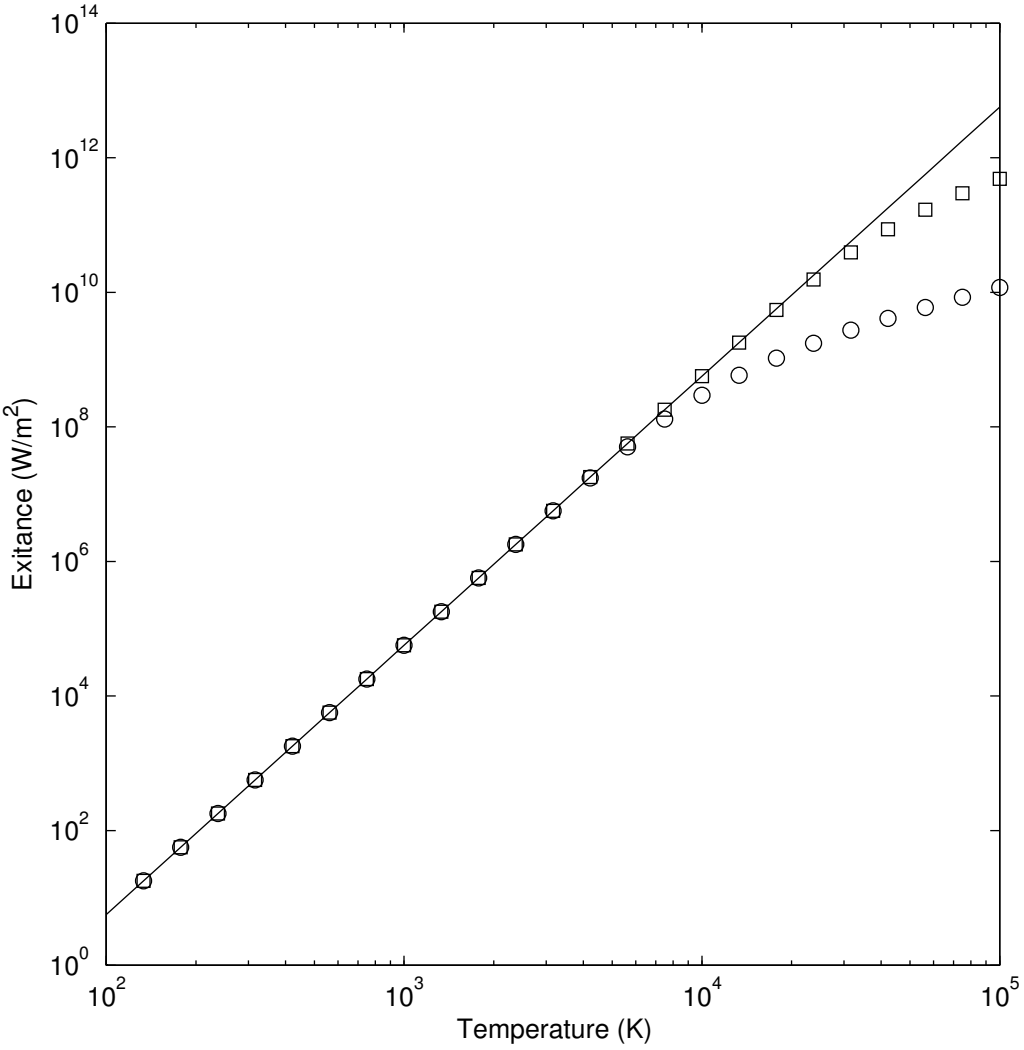

Figure 3. Comparison of `pyrosim` calculations to the Stefan-Boltzman law. Two calculations are shown, with integration from infinite wavelength to 0.400 μm (circles) and 0.100 μm (squares). The solid line shows the theoretical result (Equation 8).

straight line in a log-log plot. This discrepancy occurs because `pyrosim` integrates to finite energy maximum (minimum wavelength), and emission below this wavelength increases at high temperatures. Reducing the cutoff wavelength from 0.400 μm to 0.100 μm improves the agreement between calculation and theory, but eventually the former will drop below the latter. In practical calculations, this shortcoming is not a problem as real detectors are sensitive to a limited spectral range.

4.2 Infrared pyrometery

Consider a pyrometer with five infrared channels: 4–5 μm, 3–4 μm, 2–3 μm, 1–2 μm, and 0.7–1 μm. Each band can be represented in `pyrosim` as a constant detector response with limited wavelength range (4–5 μm, etc.) or by defining a response function to simulate actual wavelength variation; for simplicity, the former method is used here with a responsivity of 1000 V/W. Figure 4 shows calculated signal curves when the pyrometer collects light through a 1 mm diameter, lossless relay (collection over 10°) for a blackbody source. Electrical signals increase monotonically with temperature on each pyrometer channel, as expected, and the longer wavelength channels produce higher signal at lower temperatures. Shorter wavelength channels eventually exceed the longer channels, however, at sufficiently high temperature.

The curves in Figure 4 provide a sense of the attainable signals levels in a time-resolved pyrometry, where temperature changes are to be measured on sub-microsecond time scales. Specific details of such experiments might vary: more electrical gain could be used, and the sample emission would typically be much lower than unity. Despite such details, the calculations provide a rough estimate of the minimum resolvable temperature. The dashed horizontal line in Figure 4 marks a 1 mV threshold, the lowest possible signal change measurable with high-speed digitizers ($>$ 1 GHz bandwidth). The curves cross this threshold (at the nearest 5 K) at roughly 375 K, 425 K, 500 K, 650 K, and 1050 K, respectively. These intersections indicate that for measurements below 500 K, mid-infrared ($>$2 μm) are required as shorter wavelengths will be entirely inactive. Near-infrared measured measurements are not useful until at least 650 K, and not until about 1000 K can narrower wavelength ranges (0.3 μm rather than 1.0 μm) be used. High-speed mid-infrared measurements are not technically straightforward, nor are near-infrared measurements at substantially higher gain levels ($\gg 10^4$ V/W), which makes time-resolved pyrometry below 1000 K very difficult.

Although signal levels rise with temperature for all channels in this hypothetical pyrometer, the rate of signal increase diminishes above the detection threshold. For example, the 4–5 μm channel signal varies from over three orders of magnitude between 200 K to 400 K, but the next three decade change takes place over 1000 K. This indicates that each channel is most sensitive to temperature just after crossing the measurability threshold, after which point other factors (such as emissivity) play an comparable or greater role in measured signal than temperature. This effect is caused by the variation of peak blackbody radiance with temperature (Wien's law): [3]

$$\lambda_{\max} \times T = 2898 \ \mu\text{m}\cdot\text{K} \quad \text{(radiance)} \tag{9}$$

which places a higher fraction of emitted power at shorter wavelengths. For example, the

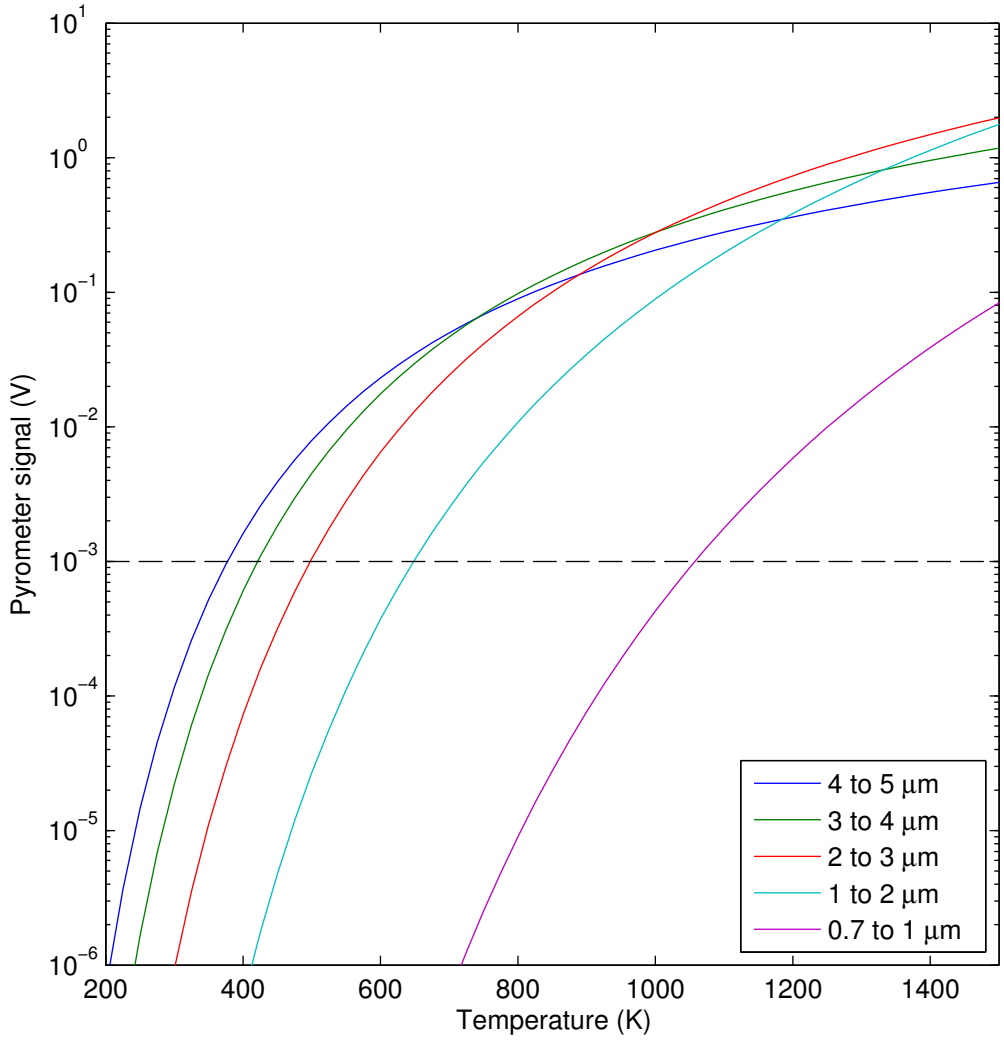

Figure 4. Infrared pyrometry calculations

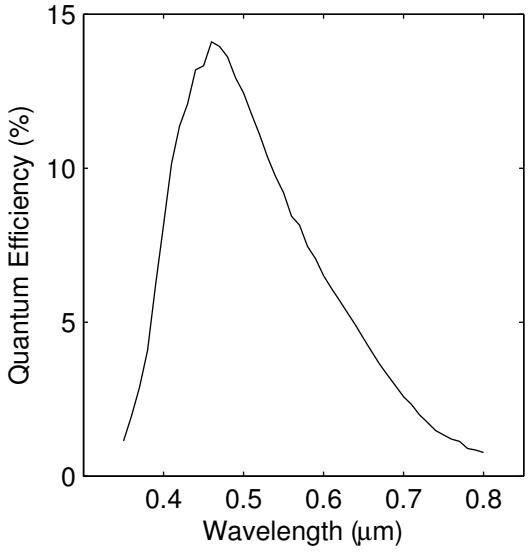

Figure 5. Quantum efficiency of the S20 photocathode

blackbody peak is at 4 μm for a temperature of 724 K, which corresponds to the reduced sensitivity of the 4–5μm channel in Figure 4 above 800 K.

4.3 Visible pyrometry

Now consider a high-speed temperature measurement using a streaked pyrometer [4]. In such a measurement, light collected from sample is dispersed spectrally by a diffraction grating and temporally by a streak camera. The output of the streak camera is coupled to a detector array (typically a CCD). Several conversions occur in this process.

1. Photons from the diffraction grating strike the photocathode of the streak camera, generating electrons.
2. These electrons accelerate across the streak camera and strike a phosphor, creating new photons.
3. Photons emitted by the phosphor may be amplified by an image intensifier (optional), which involves another set of conversions from photons to electrons and back again.
4. Photons from the phosphor (or image intensifier) strike the detector array, creating electrons that are counted and recorded.

The number of counts on a particular detector element is thus related to the photon flux on a corresponding region (accounting for magnification, distortion, etc.) of the streak camera's photocathode. Various losses/gains and nonlinearities may occur in transformation of input

photons to detector counts, much of which is beyond the scope of this report. However, the spectral variation in quantum efficiency (number of electrons generated per photon) at the photocathode will be considered in the following example. Figure 5 shows the characteristic variation for the S20 photocathode used in many streak camera measurements.

Suppose that a streaked pyrometer is configured such that each detector element receives light from a 5 nm interval using fiber coupling as the previous example (1 mm diameter, 10° maximum angle). Figure 6 shows the calculated count levels from blackbodies at several different temperatures. The curves are generated by multiple calls to `pyrosim`, calculating the photon flux at all specified temperatures for a specific wavelength range (*e.g*, 0.400–0.405 μm) on each call, as illustrated in the following MATLAB code.

```
temperature=[2000 3000 4000 8000 16e3 32e3];
dx=0.005;
min_wavelength=0.350:dx:0.775;
max_wavelength=min_wavelength+dx;
wavelength=(min_wavelength+max_wavelength)/2; % central wavelength
N=numel(min_wavelength);
photons=zeros(numel(temperature),N); % preallocation optional
for n=1:N
    [~,photons(:,n)]=pyrosim('temperature',temperature,...
        'min_wavelength',min_wavelength(n),...
        'max_wavelength',max_wavelength(n),...
        'num_wavelength',500);
end
```

Each row of the array `photons` contains an emission spectrum, in units of photons per second, for detector elements centered at the values of `wavelength`. Photocathode response can be accounted for by specifying a two-column text file containing the quantum efficiency as the relay function.

```
electrons=zeros(numel(temperature),N); % preallocation optional
for n=1:N
    [~,electrons(:,n)]=pyrosim('temperature',temperature,...
        'min_wavelength',min_wavelength(n),...
        'max_wavelength',max_wavelength(n),...
        'num_wavelength',500,...
        'relay','NSTecQE.txt');
end
```

Both calls to `pyrosim` were used in Figure 6 to estimate the count rates for an ideal photocathode (dashed lines) and a characteristic S20 photocathode (solid lines).

At least 100–1000 counts/ns are necessary for pyrometry measurements with a 1 ns exposure times, since background levels tend to be hundreds of counts (per detector element).

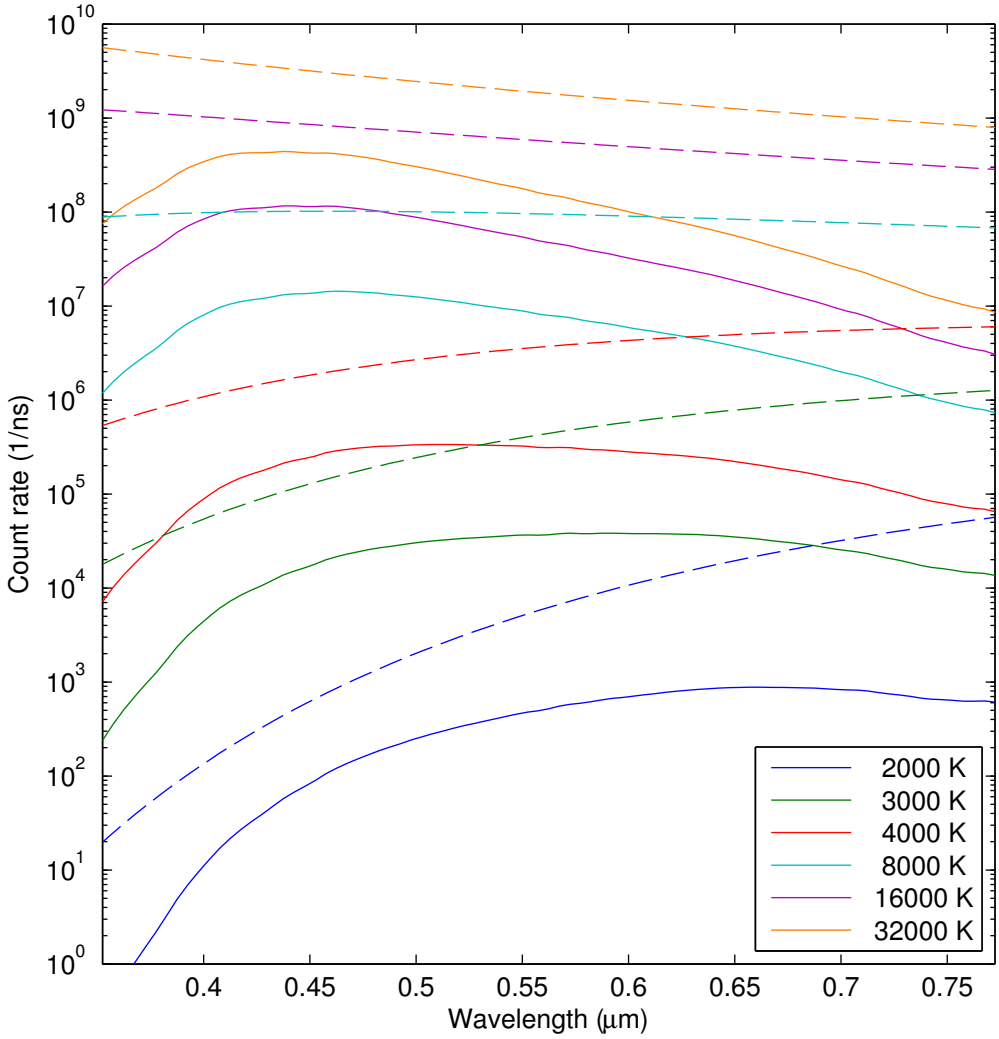

Figure 6. Visible pyrometry calculations (5 nm collection). Dashed lines indicate the photon flux at the photocathode; solid lines show the electron flux generated by the S-20 photocathode.

Figure 6 indicates that a 2000 K blackbody almost reaches this threshold, but falls short of being measurable after accounting for photocathode efficiency. Blackbody temperatures of 3000 K or more would be easily measurable with this exposure and spectral range, though temperatures beyond 4000 K would require attenuation or sub-nanosecond exposures to prevent saturation.[2]

The blue side of the count spectrum is heavily influenced by the photocathode's quantum efficiency, creating an artificial maximum in the visible region. The actual maximum count rate is defined by a variant of Wien's law: [3]

$$\lambda_{\max} \times T = 3662\ \mu\text{m}\cdot\text{K} \quad \text{(photon radiance)} \tag{10}$$

Real blackbody peaks occur in the visible between 5200 K and 9200 K; temperatures above this range peak in the ultraviolet and x-ray regions. Reduced sensitivity of a visible pyrometer is evident in similarity in the 16,000 and 32,000 K spectra. Though the latter is much hotter, the curves have similar same shapes, which could be attributed to emissivity differences rather than temperature in a pyrometry measurement.

5 Summary

The design of an optical pyrometry depends on the temperature of interest, how radiation is collected from the sample, and the detector(s) used to measure that radiation. The `pyrosim` program offers a convenient way to model each stage of a pyrometer, yielding signal estimates commensurate with the level of system characterization. Calculations with this program illustrate the competition between low temperature operation and high temperature sensitivity: long wavelength measurements can sense lower temperatures than short wavelength measurements, but become less sensitive as the the blackbody peak moves to shorter wavelengths.

References

[1] Plank, M. On the law of distribution of energy in the normal spectrum. *Annalen der Physik* **4**, 553 (1901).

[2] D.P. DeWitt and G.D. Nutter, editor. *Theory and Practice of Radiation Thermometry.* Wiley, New York, (1988).

[3] E.L. Dereniak and G.D. Boreman. *Infrared detectors and systems.* John Wiley & Sons, (1996).

[4] G. Dunham, J.E. Bailey, A. Carlson, P. Lake, and M.D. Knudson. Diagnostic methods for time-resolved optical spectroscopy of shocked liquid deuterium. *Review of Scientific Instruments* **75**, 928 (2004).

[2] Most detector arrays are limited to a 16-bit (65,536 levels) count range.

DISTRIBUTION:

2 National Security Technologies
Las Vegas Operations
P.O. Box 98521
Las Vegas, NV 89193
Attn: S. Becker

2 National Security Technologies
Los Alamos Operations
P.O. Box 809
Los Alamos, NM 87544
Attn: A. Iverson

2 National Security Technologies
Special Technologies Laboratory
5520 "B" Ekwill Street
Santa Barbara, CA 93111
Attn: G. Stevens

2 Lawrence Livermore National Laboratory
7000 East Ave.
Livermore, CA 94550
Attn: N. Holmes

2 Los Alamos National Laboratory
P.O. Box 1663
Los Alamos, NM 87545
Attn: D. Holtkamp

1	MS 1195	S.C. Alexander, 1646
1	MS 1195	T. Ao, 1646
1	MS 1196	J.E. Bailey, 1677
1	MS 1195	J.-P. Davis, 1646
2	MS 1189	M.P. Desjarlais, 1640
1	MS 1195	J.L. Brown, 1646
5	MS 1195	D.H. Dolan, 1646
1	MS 1454	D. Farrow, 2554
2	MS 1189	D.G. Flicker, 1646
1	MS 1195	M.D. Furnish, 1646
1	MS 1193	R.G. Hacking, 16561
1	MS 1454	B. Jilek, 2554
1	MS 1195	M.D. Knudson, 1646
2	MS 1195	G.T. Leifeste, 1647
2	MS 1454	L. Minier, 2554
1	MS 1193	S.L. Payne, 16561

1	MS 1195	W.D. Reinhart, 1647
2	MS 1196	G.A. Rochau, 1675
1	MS 1195	S. Root, 1646
1	MS 1195	T.J. Vogler, 9042
1	MS 1195	J.L. Wise, 1646
1	MS 0899	Technical Library, 9536 (electronic copy)

This page intentionally left (almost) blank.

Sandia National Laboratories